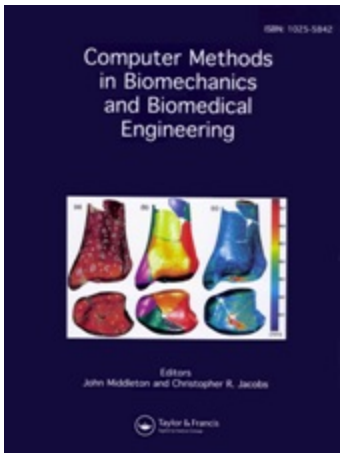

Validation of a numerical model for the mechanical behavior of a Continuous Positive Airway Pressure mask

Journal:	*Computer Methods in Biomechanics and Biomedical Engineering*
Manuscript ID	GCMB-2021-0143.R1
Manuscript Type:	Research Article (5500 words)
Date Submitted by the Author:	n/a
Complete List of Authors:	Genna, Francesco; University of Brescia, Dept. Civil Engrg. Lopomo, Nicola; University of Brescia, Dept. Information Engrg. Savoldi, Fabio; University of Brescia, Dept. Medical Surgical Specialties, Radiological Sciences and Public Health
Keywords:	Finite Element analyses, unilateral contact, contact pressures

Validation of a numerical model for the mechanical behavior of a Continuous Positive Airway Pressure mask

Francesco Genna
(Dept. Civil Engrg., University of Brescia, via Branze 43, 25123 Brescia, Italy.
Corresponding Author: phone +39 030 3711275; fax +39 030 3711312;
email: francesco.genna@unibs.it)

Nicola Francesco Lopomo
(Dept. Information Engrg., University of Brescia, 25123 Brescia, Italy)

Fabio Savoldi
(Dental School, Dept. Medical Surgical Specialties, Radiological Sciences and Public Health, University of Brescia, Piazza Spedali Civili 1, 25123 Brescia, Italy.
Orthodontics, Division of Paediatric Dentistry and Orthodontics, Faculty of Dentistry, The University of Hong Kong, Prince Philip Dental Hospital, 34 Hospital Road, Sai Ying Pun, Hong Kong S.A.R.)

This work is dedicated to the memory of Professor Pier Luigi Sapelli

Abstract

Finite Element models (FEM) are developed for the analysis of the contact pressures exerted by a Continuous Positive Airway Pressure (CPAP) mask applied to a dummy head. This is seen as a preliminary step in the analysis of the mechanical effects of CPAP masks applied to human faces, such as recently employed for the care of COVID-19 patients, or other purposes. These mechanical effects can range from negligible, in the case of correct positioning, sufficiently light tension in the headgear, correct mask design, etc., to the possible development of device-related pressure ulcers and/or dentofacial deformations, especially in children. The results of Finite Element analyses are compared, for their validation, with experimental ones. The numerical analysis tool appears able to predict, at an acceptable cost, both the intensity and the area distribution of the contact pressures, as well as the force-displacement relationship occurring in the headgear. This might help the design and the production of more effective and tolerable CPAP masks.

Key terms

Finite Element analyses; unilateral contact; contact pressures.

Introduction

Continuous Positive Airway Pressure (CPAP) masks are adopted to treat several medical conditions including respiratory failure associated with COVID-19 infection [13] and obstructive sleep apnea [12]. The standard use implies their placement over the face of the subject, tensioning and fastening a headgear around the head, and keeping the device on under air pumping through an intake tube [8]. The tension in the headgear bands, necessary both to keep the mask in position and to guarantee a good sealing so as to limit air leakage, can however be the source of possibly severe problems deriving from the long duration and the relatively high intensity of the involved forces, including device-related pressure ulcers [6] and dentofacial deformities [17].

In spite of the importance of this problem, especially with the recent (starting with year 2020) surge in CPAP side effects related to extensive use during the COVID-19 pandemic [6], little in-vivo work appears to have been devoted to the study of the mechanics of CPAP masks or other masks used for noninvasive ventilation [3, 4, 14, 18]. Even the choice of the tension force in the headgear is routinely done by trial-and-error procedures [18].

In-vivo experimentation is difficult to pursue, because of issues both in defining controlled load conditions and in positioning the necessary sensing solutions. The possibility of a numerical approach to this problem seems therefore of interest, as already proposed for respirators and other personal protective equipment [5, 9]; some work has given preliminary indications in this respect [1, 11, 14], but the field appears in the need of validated studies. On the other hand, it is apparent that the problem under consideration might present a rather formidable obstacle also in numerical terms, because of several sources of difficulties. Among these, the different geometrical scales of the global mask size and its thicknesses, the much different stiffnesses of the materials involved, the presence of large displacements and possibly of large strains in the soft parts, the presence of unilateral contact with friction, and the coupling of solid with gas mechanics.

In this work no attempt was made to consider coupled solid-gas models. Only the mechanical aspects of the problem were taken into consideration, and a Finite Element (FEM) model in terms of Solid Mechanics was developed, aimed at computing the mechanical response due to a CPAP mask subjected to its typical loading conditions. Only one type of mask was selected as a standard prototype. The FEM model developed aimed at overcoming all the difficulties listed above and it produced acceptable results. In order to have a validation of these results, laboratory tests were performed in an in-vitro experimental setup, in which a dummy head was adopted and equipped with contact pressure sensors placed in four locations of main interest. The complete details of these (and other) tests are reported elsewhere [10]; here only the main results are recalled and adopted for comparison with the numerical ones.

Both force-displacement curves and contour plots of the contact pressures between mask and dummy head are presented. The indication was obtained that, despite the difficulty of this problem, numerical analyses could be employed both to optimize the geometrical and material details of CPAP masks and to analyze their behavior under loading.

Further work is in progress with the aim of introducing into the numerical simulations a better correspondence with a real clinical situation.

Materials and Methods

Experimental

The full details of the laboratory tests are described elsewhere [10]. For lack of space, here we limit ourselves to the essential information required to validate the numerical simulations.

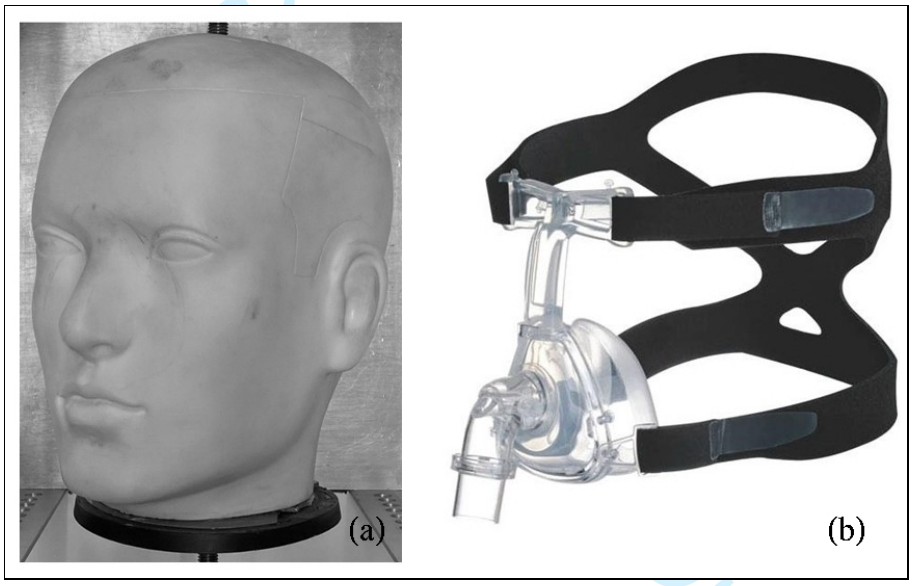

Figure 1: (a) adopted dummy head; (b) CPAP mask with headgear. During all the tests the air intake tube (protruding and pointing downwards from the center of the anterior surface of the mask) was removed.

Figure 1 shows both (a) the considered commercially available dummy head (PlusSign, P. R. of China), made by PVC and filled with extra-hard dental plaster, and (b) the CPAP mask with the headgear (size M, iVolve N2, BMC Medical, P. R. of China). The mask is made by a polycarbonate frame, with thin soft silicone rubber cushions for the contact with the skin. The mask headgear consists of two bands, made of one layer of unbroken loop fabric (UBL) on the outer surface, one layer of styrene butadiene copolymeric rubber (SBR) in the middle layer, and one layer of nylon (70D) in the inner surface. Velcro connectors are attached to the extremities of each band, to allow the connection to the mask frame at the forehead level and at the nasal level (symmetrically on both sides).

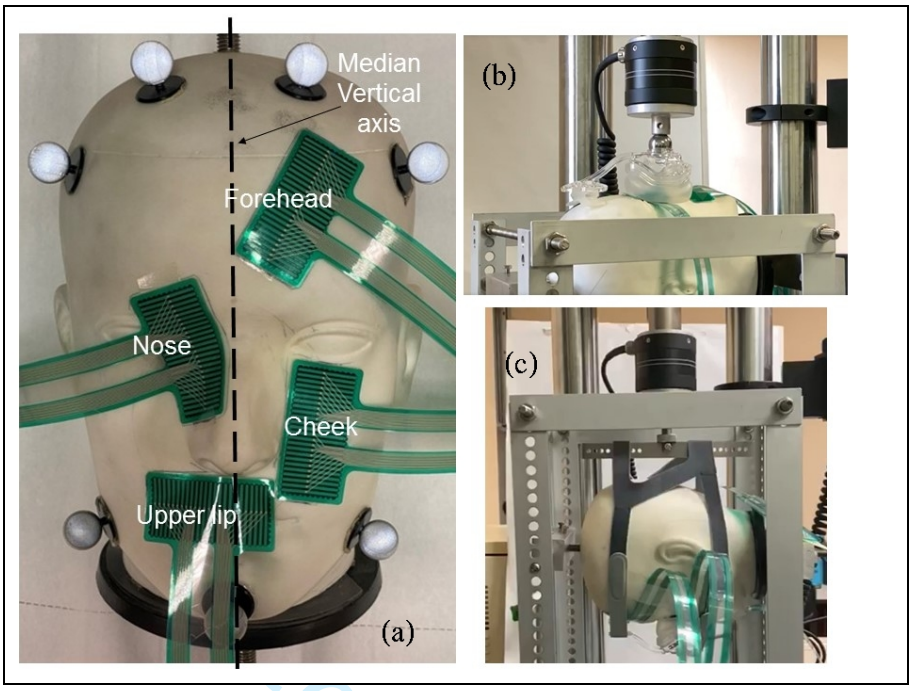

Figure 2: (a) location of the contact pressure sensors applied to the face of the dummy head; (b) simplified compressive loading setup; (c) headgear tension loading setup.

The dummy head was bolted to an aluminum frame at the top and bottom points of the head on its median vertical axis, intersecting the coronal and the sagittal planes (Figure 2 a). Four contact pressure sensors (mod. 4201, Tekscan, USA) were applied to the dummy head face, and their precise relative locations were acquired by means of a marker-based optoelectronic system (SMART-DX 400, BTS Bioengineering, USA). In the following, reference will be made to the four positions of the pressure sensors as “upper lip”, “cheek”, “nose”, and “forehead”, as shown in Figure 2 (a).

Two different sets of tests were performed (see Figure 2, images b and c). In a first one, the aluminum frame with the dummy head was positioned in the testing machine (Microtester 5848, Instron, USA) with the face pointing upwards. The CPAP mask, with no headgear attached, was positioned on the top of the face, and a steel sphere of 25.4 mm diameter was placed in the mask hole for the air intake. The steel sphere was loaded by a vertical compressive (downward) force of 20 N applied with a linear increase in 20 sec. The purpose of this test was of having available results associated to the simplest possible boundary conditions, for an easy comparison between experimental and numerical results.

The second test was meant to simulate the tensioning of the headgear and the consequent pressure development on the face surface under a more realistic loading condition. In this case the dummy head faced downwards, the CPAP mask was positioned underneath the face, and the headgear was attached and closed around the head. A steel bar was then inserted between the back of the head and the headgear bands. It was then connected to the top clamp of the testing machine. An initial loading step was prescribed which

put the headgear into tension by a total force of 2 N. Thereafter, a force-controlled test was made by applying a tensile (upward) force of 20 N in 60 sec.

In both tests the forces and the displacements were recorded, as well as the contact pressures at the four pressure sensors.

Numerical

The geometry of the solids depicted in Figure 1 was acquired by means of an optical laser-scanner device (CRONOS 3D, Open Technologies, Italy), and the produced point cloud STL file was transformed into a 3D solid SAT file, suitable as an input for the adopted FEM code, by means of a graphical software (Geomagic Studio, v2014, 3D Systems, USA). The small thickness of all the mask parts had two consequences: (i) a somewhat unsatisfactory scansion, with loss of detail with regard to the thicknesses and the internal parts; and (ii) the choice of modelling all the mask parts as thin shells, with different thicknesses to be assigned a-posteriori.

The high elastic stiffness of both the PVC material of the dummy head and the polycarbonate material of the mask frame, with respect to that of both the silicone rubber cushion and the headgear parts of the mask, led to the choice of defining the stiffer parts as perfectly rigid during the FEM analyses. This prevented the ill-conditioning of the stiffness matrices, avoided analysis failures, but did not introduce any loss of accuracy in the prediction of the mechanical quantities of interest. Likewise, also the dummy head was modelled as a fully rigid shell surface.

All the analyses were run adopting the commercial FEM code ABAQUS [7]. Implicit Dynamics was adopted, in order to capture the large rigid, or quasi-rigid, body motions implied by the problem. The Hilber-Hughes-Taylor time integration algorithm was employed, with the default value for the selective numerical damping coefficient $\alpha = -0.05$. All the analyses were run in the regime of large displacements and large strains.

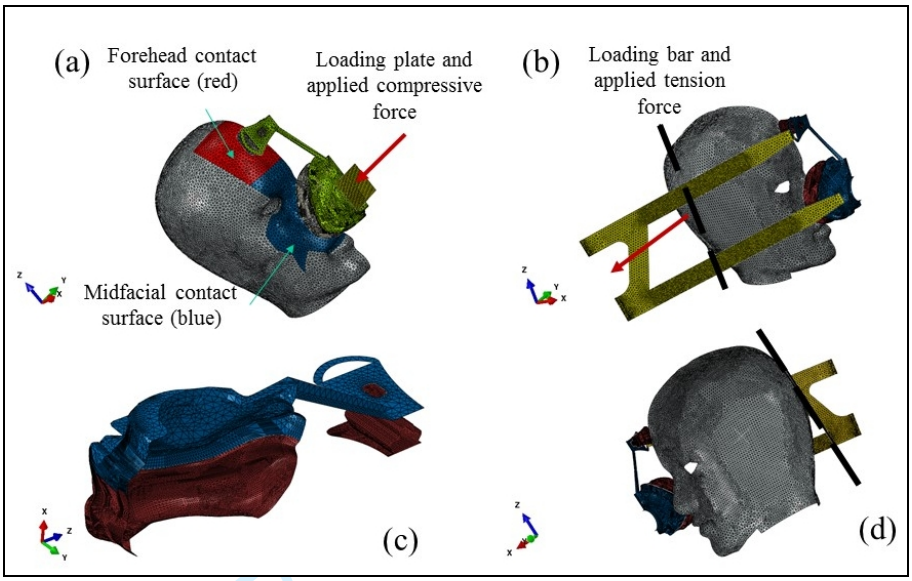

Figure 3: FEM mesh, contact surfaces, and loading conditions for the simplified compressive loading case (a) and the headgear tension loading case (b seen from the outside, and d seen from the inside of the head surface). Image (c) shows an enlargement of the CPAP mask: the polycarbonate part is plotted in blue, the silicone rubber in red.

All the surface geometries were imported into ABAQUS from the obtained SAT files. Only one half of the problem was studied, exploiting the theoretical symmetry with respect to the sagittal (median, x–z, in the numerical models, see Figure 3) plane. The thicknesses were defined for each deformable surface, trying to match the measured ones for the various parts of the mask.

The elastic properties of the silicone rubber were obtained from laboratory uniaxial tests on small samples. These tests showed that, in the strain range of interest, the silicone rubber did behave in an almost linear elastic fashion (see [10] for complete details). As a consequence, a linear elastic material model was adopted for the silicone rubber, with Young modulus equal to $E = 2$ MPa. The Poisson coefficient ν was taken equal to $\nu = 0.4$. The mass density ρ of the silicone rubber was taken equal to $\rho = 1.2e{-}9$ N sec/mm^4.

The overall elastic properties of the headgear portions were also obtained from uniaxial tests on small portions of the bands. The Young moduli were $E = 2$ MPa for the thin parts of the bands, and $E = 3$ MPa for the thicker parts where the Velcro fasteners exist. The Poisson coefficient was $\nu = 0.45$. The mass density of the headgear material was $\rho = 9.5e{-}10$ N sec/mm^4.

A Rayleigh material damping was introduced, with only the stiffness-proportional coefficient $\beta_R = 0.001$ different from zero.

The mask was initially placed at a small distance from the dummy head, since it was practically impossible to define a-priori a precise initial contact configuration between the two parts. A suitably designed initial loading step was defined in all the models, in order to let the code automatically find such an initial configuration.

Several surfaces of unilateral contact were defined in the models. The main ones were (i) the top (frontal) part of the dummy head, in possible contact with the top silicone part of the mask; (ii) the midfacial part of the dummy head, in possible contact with the bottom silicone part of the mask; (iii) the surfaces of the headgear bands and the corresponding ones on the dummy head (see Figure 3). Further contact surfaces were defined between different silicone portions of the top part of the mask which, upon loading, could touch each other. A standard Coulomb friction model was assumed, with friction coefficient $\mu = 0.8$ for the contact between silicone and PVC, and $\mu = 0.1$ for the contact between the headgear material and the PVC.

The two loading setups of the experiments were considered. The full sets of loading steps and relative applied forces and other boundary conditions were as follows, for the two different considered situations.

1. Simplified compressive loading condition. The rigid dummy head was fully fixed to the reference system. Symmetry conditions with respect to the *x*–*z* plane were enforced to the CPAP mask ($u_y = r_x = r_z = 0$ on the lines lying on the symmetry plane, *u* denoting nodal displacements and *r* nodal rotations). A first loading step applied gravity to the mask in the negative *x* direction, in order to let it find a first contact configuration with the dummy head. In the numerical model, the compressive force exerted by the testing machine on the steel sphere was applied to a steel plate in unilateral contact with the surface of the air intake hole of the mask. During the first gravity loading step, also the self-weight of the loading sphere was considered, so that also the loading plate, in the model, could find a stable contact configuration with the mask before applying further loading. A concentrated compressive force, increasing linearly with time from $f_x = 0$ to $f_x = -10$ N, was then added to the center point of the loading plate, to represent a 20 N compressive loading on the full mask.

2. Headgear tension loading condition. The headgear, modelled as a thin shell with the relevant thicknesses, was added to the model, as shown in Figure 3 (b, d). The two ends of the headgear closest to the mask were constrained to follow the motion of the corresponding hooks in the rigid (polycarbonate) part. A rigid shell, representing the steel element adopted in the laboratory tests to pull the headgear (Figure 3 b, d), was also added to the model. The dummy head was fully fixed to the reference system. Symmetry conditions with respect to the *x*–*z* plane were enforced to the CPAP mask. In a first loading step, gravity was prescribed to the mask in the negative *x* direction, in order to obtain a first contact with the dummy head surface. In a second loading step, the two free ends of the headgear were subjected to prescribed displacements in the *y* direction only, so as to bring them on to the symmetry plane and force a curvature of the headgear bands around the dummy head. A tensile concentrated force of 1 N (the pre-loading of 2 N applied in the test) was applied next to the rigid shell representing the loading steel bar, and the final loading step added a concentrated tensile force of 10 N. Both forces varied linearly with time from zero up to their maximum value, and were applied to the loading rigid element in the negative *x* direction, so that this

element first reached contact with the headgear ends and then started pulling them, thus replicating the experimental setup, when a final total pulling force of 22 N was applied to the mask.

The deformable silicone rubber and headgear parts were discretized using linear triangular shell elements with finite membrane strains (element S3 in the ABAQUS terminology). The choice of linear (3 noded) elements is almost mandatory to have a good behavior in terms of contact forces. All the rigid parts were discretized using triangular linear (3 noded) rigid shell elements (R3D3 in ABAQUS notation). The average element size in both models was of about 2 mm, with larger elements in the rigid parts and five times smaller ones in the silicone rubber zones undergoing large curvatures, where the main quantities of interest were computed. The model with no headgear had about 240000 degrees of freedom, while the model with the headgear had about 380000.

Results

Experimental

1. Simplified compressive loading condition. Figure 4 reports the force-displacement curves obtained for both the experimental loading conditions under 20 N forces; the curve produced by the simplified loading setup is marked by black circles.

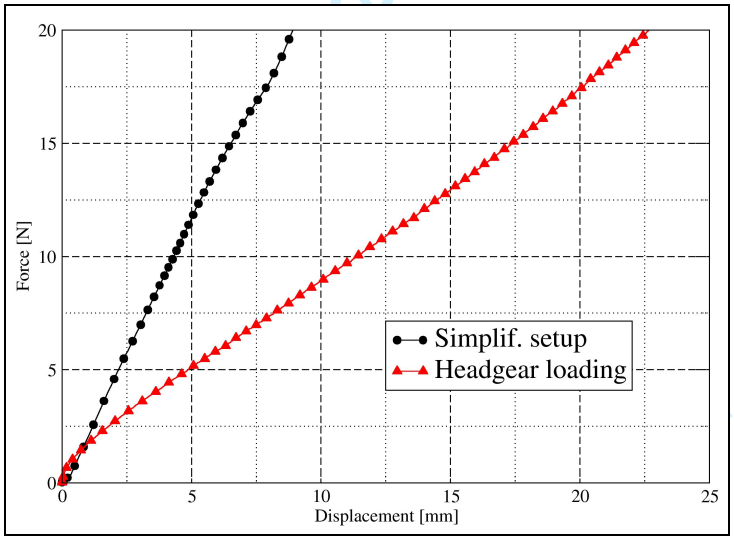

Figure 4: force-displacement curves recorded during the tests. The stiffer one, with black circles, was produced by the simplified compressive loading setup; the less stiff one, with red triangles, by the headgear tension loading setup.

The “artificial” loading condition of the simplified compressive setup puts most of the pressure on the upper lip and cheek regions of the face, where peak pressure values of the order of 0.08 MPa (cheek) or 0.063 MPa (upper lip) occur. The nose and forehead sensors did not record much information (see also Figure 6 and Table I).

2. Headgear tension loading condition. The force-displacement curve recorded for this loading condition is shown in Figure 4 with red triangles. Even though the total applied force was the same as in the first loading case, the different mode of application produced more widespread pressures (see also Figure 8 and Table II).

Numerical

1. Simplified loading condition, 20 N compressive force. In the numerical simulations a first difficulty was the individuation of the precise location of the mask with respect to the face. As said, the mask was left at a small distance from the face, and a gravity loading step was defined in order to let the code find the initial contact configuration. The simple loading condition of this case enabled us to perform extra runs varying both the inclination of the mask with respect to the head face and the mask positioning along the *z* axis, in order to check the possible influence of these geometrical factors on the computed response.

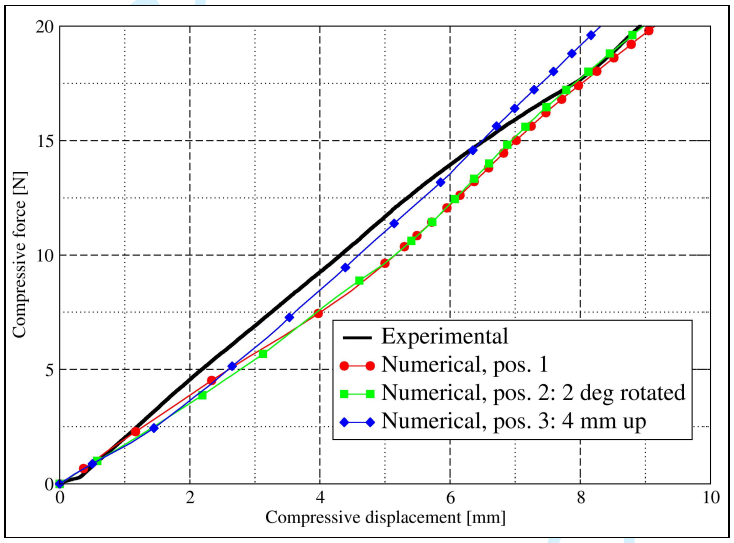

Figure 5: simplified compressive loading condition. Comparison among force-displacement curves: experimental (solid black) and numerical (in color, with symbols). Different symbols correspond to different initial locations of the CPAP mask, as explained in both the legend and the text.

Figure 5 shows the force-displacement curves obtained numerically for three different initial positionings of the mask, together with the experimental result of Figure 4. In position 1 the lower mask edge touched the upper lip, and there was no inclination with respect to the dummy head, i.e., the plane passing through the air intake hole was parallel to the *y*–*z* plane. Position 2 was rotated from position 1 by 2 degrees around the *y* axis, bringing the bottom edge of the mask closer to the head upper lip. Position 3 was 4 mm apart from position 1 in the positive *z* direction, towards the top of the head, with no inclination. There is not much difference among the numerical results, even though the best fit with the final displacement value is given by the first two curves.

Figure 6 shows the comparison between the experimental and the numerical contact pressures in the four considered locations for the mask configuration of position 1.

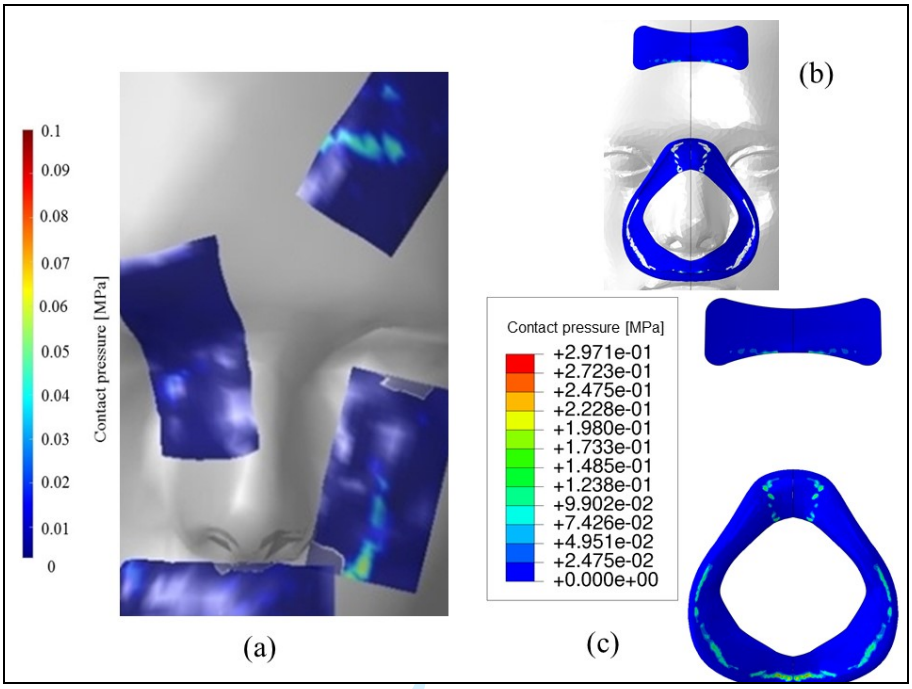

Figure 6: simplified compressive loading condition. Comparison between the experimental (a) and the numerical (c) contact pressure contour plots. Plot (b) shows the location of the surfaces on the dummy head in the numerical model.

Also for the contact pressures there is very little difference among the results associated to the three different initial positionings of the mask. In all the following, only position 1 will be considered.

	Experimental			Numerical		
	Peak press. [MPa]	**Avg. press.** [MPa]	**Contact area** [mm^2]	**Peak press.** [MPa]	**Avg. press.** [MPa]	**Contact area** [mm^2]
Upper lip	0.063	0.017	425	0.3	0.046	76
Cheek	0.08	0.025	195	0.16	0.029	179
Nose	0.026	0.01	150	0.18	0.03	80
Forehead	0.011	0.0055	145	0.14	0.013	108

Table I: experimental vs numerical contact pressures and areas for the simplified loading case. “Avg. press.” stands for “Average pressure” over the pressure sensor.

The numerical result seems at a difference, with respect to the experimental one, in two main respects: (a) higher average pressures in the upper lip and nose regions and (b) higher peak pressure values at all the considered locations.

Table I summarizes this comparison in terms of peak and average pressure values and contact areas. It is worth observing that the most reliable comparison is for the cheek sensor only, because (i) the upper lip sensor, which covered the totality of the upper lip, was located in a zone of strong

curvature of the facial surface; (ii) the nose sensor was also located in a zone of strong curvature and inclination leading to a non-perpendicular load application. Both upper lip and nose sensors did not follow accurately such a curvature. The forehead sensor (iii) did not cover the whole contact surface between mask and head, because of difficulties due to both the presence of the cables and the overlapping with other sensors.

In the cheek sensor zone both the contact surface and the average contact pressure were correctly predicted by the numerical analysis. The computed pressure peak, instead, was twice the one given by the sensors. Reasons for this will be given in the next section.

2. Headgear tension loading condition, 20 N force. Figure 7 shows the comparison between the experimental and numerical force-displacement curves relative to the loading device.

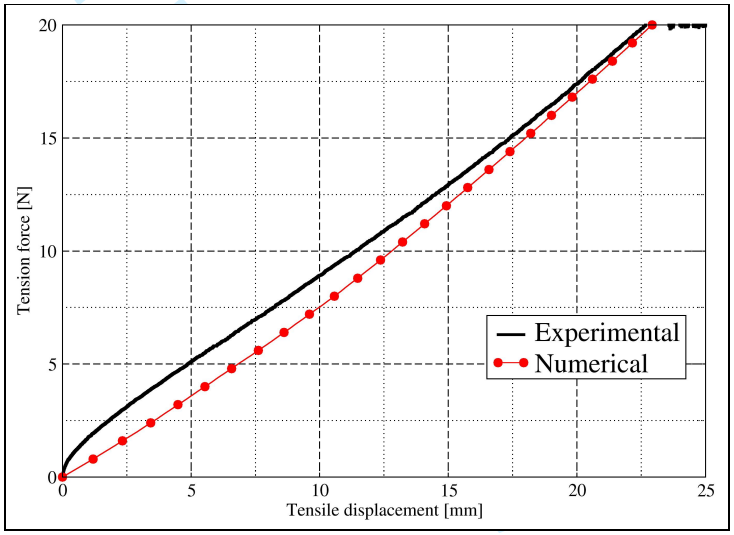

Figure 7: headgear tension loading condition. Comparison between force-displacement curves: experimental (solid black) and numerical (with red circles).

The details of this curve depend now both on the contact development details and on the geometrical/mechanical properties of the headgear bands. Therefore, a perfect coincidence of the curves of Figure 7 should not be expected, in view of the difficulty associated to correctly modeling both these factors. Nevertheless, the numerical prediction is quite reasonable; the difference in the initial global stiffness could also be ascribed to the fact that in the experimental setup the headgear bands were under some tension before the application of any load, whereas in the numerical analysis they start fully unloaded.

Figure 8 shows a comparison of the contact pressures, and Table II shows their significant numerical values.

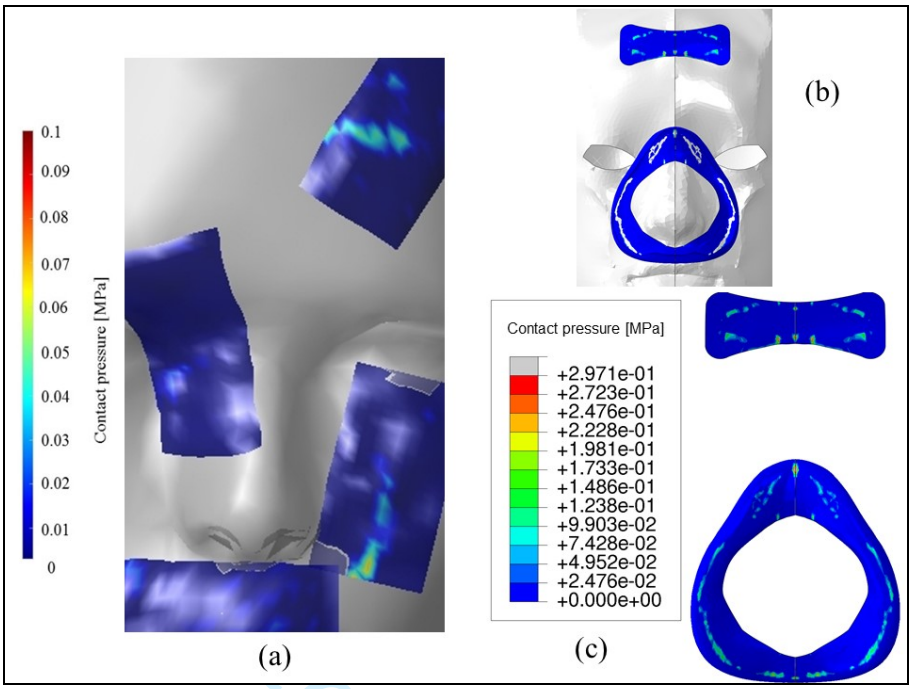

Figure 8: headgear tension loading condition. Comparison between the experimental (a) and the numerical (c) contact pressure contour plots. Plot (b) shows the location of the surfaces on the dummy head in the numerical model.

	Experimental			Numerical		
	Peak press. [MPa]	**Avg. press.** [MPa]	**Contact area** [mm^2]	**Peak press.** [MPa]	**Avg. press.** [MPa]	**Contact area** [mm^2]
Upper lip	0.023	0.009	360	0.30	0.033	420
Cheek	0.069	0.02	147	0.15	0.025	168
Nose	0.023	0.009	130	0.18	0.023	102
Forehead	0.0055	0.0145	242	0.18	0.021	309

Table II: experimental vs numerical contact pressures and areas for the headgear loading case.

The redistribution of the pressures towards the forehead with respect to the previous loading case, due to the different loading modality, is apparent in both the experimental and numerical results. Once again, in terms of numerical values the only meaningful comparison can be made for the cheek sensor, where the numerical predictions appear acceptable except for the peak pressure value.

Discussion

1. Experimental, simplified loading condition. As shown in [10], all the important phenomena occur under essentially elastic (reversible) conditions. This confirms that the numerical analyses, for this problem, can be performed adopting linear elasticity for all the materials.

2. Experimental, headgear loading condition. Once again, linear elasticity of the problem is suggested by the result of Figure 4, in which the global

stiffness remains practically constant up to the maximum force. Unlike the previous case, in which the loading condition was easy to be reproduced in a numerical model, and in which the displayed global stiffness depended only on the stiffness of the mask and the contact details, in this case the force-displacement curve is very much affected by the global stiffness of the headgear, more difficult to be accurately reproduced in numerical models. The global stiffness of the problem, for this case, is about 2.5 times smaller than in the first case, which confirms the important effect of the headgear on this quantity.

In general, the experimental results have probably been adversely affected by the relatively high stiffness of the pressure sensors, which limited their full adaption to the surfaces with higher curvature of the dummy head and therefore produced pressure values likely different from those to be expected on the face surface itself. The irregular anatomy, together with the need to cover a relatively large area, posed difficult experimental conditions. As said in the previous section, the most reliable pressure data could be expected in the cheek sensor.

It is interesting to observe that in all the sensors the contact zones are somewhat localized, which could be a consequence of the high stiffness of both the sensors and the dummy head, but which is also expected to be a consequence of a non-optimal design of the silicone rubber part of the mask. The measured pressure values, for the “realistic” loading case, have peaks of 0.07 MPa, and average values around 0.02 MPa, under a total force of 20 N. It is unlikely that such a high force value might be clinically applied to a headgear band for a long time, but values greater than 5 N, up to maybe 10-15 N, could be expected [14]. Accordingly, peaks of pressure of the order of 0.05 MPa, for the setup considered here, should be considered realistic. It is not yet easy to say if pressure values of 0.05 MPa would have any consequence in terms of possible soft tissue injuries or on the craniofacial development of human beings [2]. At a first glance, however, one could argue that this is a rather high value for the simple stabilization of the device, and that the mask design should aim at reducing it to just what is clinically required, possibly through a widening of the contact zone [14]. Further work is needed to clarify this important point, with efforts to reproduce a more clinically meaningful situation. Some activity in this respect is currently in progress.

Another aspect related to the contact pressures and the contact surface distribution on the face is the search for a minimal air leakage during the mask usage. Analyses like these should help in designing both CPAP masks (both static morphology and dynamic fitting), and associated tension forces in the headgear bands, capable to produce full contact all around the nose with the minimum sufficient contact pressure level to avoid air leakage. The setup studied here produces many zones of no contact between mask and face, which could lead to an excessive air leakage. Of course, this setup does not represent a real clinical situation, and more studies are needed to have a good understanding of all these factors.

3. Numerical, simplified loading condition. The adopted model seems capable to correctly predict the force-displacement curve that, in this case, depends essentially on the mechanical and geometrical features of the silicone rubber part of the CPAP mask. The numerical values of the contact pressures are always higher than the experimental ones, and the contact areas smaller. As said, however, this difference is mainly due to the high stiffness of the sensors, which prevents their full adjustment to the surface of the head even under loading, thus implying a laboratory situation somewhat different from the numerical one. Only the cheek sensor is located on a reasonably flat surface, and for this sensor, where the highest pressures appear, the numerical values of both the contact areas and the average pressures are in very good agreement with the experimental ones. The peak values are not: the FEM model predicts pressure peaks about double than measured.

One should recall, in this respect, that FEM pressures are nodal values computed on discretized surfaces, where the normal vectors vary in a discontinuous way, following a non-smooth surface that may present several edges and/or vertices which in reality do not exist. The scansion and subsequent geometry conversion of both the mask and the dummy head, moreover, did produce significantly non-smooth surfaces to begin with. For these reasons, in FEM analyses of this problem contact tends to occur at isolated points or edges, especially in the presence of a fully rigid material. All this is expected to produce isolated and unrealistic high nodal pressure peak values. In general, the examination of FEM results in terms of contact pressures on the surfaces of 3D models should be approached with much caution.

Another reason for the difference among the local pressure values could be the necessity of introducing a piecewise-constant thickness of the shell elements that model the silicone rubber parts. In reality, the thickness varies in a continuous way. Another difficulty is that the free edges of the silicone part in the considered mask have a very small thickness, of the order of a fraction of millimeter, which could not be introduced in the numerical model. The local pressure values are expected to depend on all these details as well, and therefore their predicted values should always be taken with some caution.

4. Numerical, headgear loading condition. As said, now the force-displacement curve at the loading point depends much also on the properties of the headgear bands and is less meaningful than the previous case in terms of comparison between experimental and numerical results. For the contact pressures the same considerations apply as for the previous case.

Both types of analyses required some computational cost that, considering the complexity of the problem, did not exceed reasonable limits. The wall-clock time, on a Linux workstation equipped with 256 GB of RAM and an 8-core processor, and exploiting the parallel computing features of ABAQUS, was of 4 hours for the simplified loading condition and 24 hours for the headgear loading case.

In general, one should be aware of a conflict in the choice of shell elements to model the silicone rubber part of this mask. On one side shells imply a definite reduction of the computational costs with respect to a full 3D description. On the other, however, their use prevents an accurate description of the details of the problem, which may prove essential to capture the details of the contact pressures. Moreover, in the present case the necessity of introducing thickness discontinuities could produce convergence problems or anyway numerical difficulties, as well as not fully correct results, in zones where a sudden change of thickness is accompanied by strong increments of curvature. Shell elements, finally, especially under large strains and displacements, are in general of very difficult formulation, lack solid convergence properties, and are of dubious reliability, even though ABAQUS has proved for a long time to be as reliable as currently possible. The difficulties encountered during the laser scansion of the mask did force the adoption of a shell modeling. Nevertheless, the experience acquired during this study suggests that this class of problems would require a full 3D continuum type of modeling.

Conclusions

The comparison between experimental and numerical results has shown that FEM analyses are a useful tool for predicting the mechanical behavior of CPAP masks pressed in position on the face. Even though the required FEM models are fairly complex and time consuming, on their basis it should be possible both to design “optimal” mask geometries/materials and to understand what type of mask, and what specific setting, are more adequate for individual needs. It is expected, for example, that changes in the geometry of the soft silicone parts of the studied mask might improve the contact pressure distribution to reduce the risk of soft tissue injuries. Similarly, also changes in the material properties could be of help. Changes in the headgear geometry and materials, together with a better understanding of the optimal tension to be applied to it, could be considered both to improve the pressure distribution on the cranium on selected regions, and to improve the functioning of the mask. Shape and material optimization techniques could be adopted for both these purposes.

In the considered experimental setup there are clearly areas that can be improved to make the study more clinically meaningful. The use of a rigid dummy head, the presence of stiff and large pressure sensors, and the absence of air flow are all elements that on one side have allowed a relatively easy comparison with the numerical results, thus enabling one to have their validation, but on the other have limited the clinical relevance. Work is in progress to produce numerical models closer to the real in-vivo situation. A first step, currently under way, could be to consider a head made by a rigid surface covered by a soft deformable layer that simulates the soft facial tissues. More accurate cranial models, possibly including cranial sutures [15, 16], could also be considered. Finally, sophisticated models coupling solid and fluid mechanics could also be developed to have a full understanding of the mechanics involved by facial masks.

Acknowledgments

The help of Prof. C. Paganelli and Dr. L. Svanetti, of the Dental School, University of Brescia, Italy, during the experimental part of this work is gratefully acknowledged. The kind help of Prof. Giorgio Vassena and coworkers at Gexcel, Brescia, Italy, in the processing of the mask geometry, is acknowledged. The financial support of both the University of Brescia and the Italian Ministry of Teaching and Research (MIUR) is also acknowledged. The FEM code ABAQUS was run at the Department of Civil Engineering of the University of Brescia, Italy, under an academic license. The inter-departmental "Laboratorio di Fisiologia Clinica Integrativa" of the University of Brescia is acknowledged for the technologies used for measuring the contact pressures.

References

[1] Barros, L. S., P. Talaia, M. Drummond, and R. Natal-Jorge. Facial pressure zones of an oronasal interface for noninvasive ventilation: a computer model analysis. Jornal Brasileiro de Pneumologia, 40(6), 652-657, 2014.

[2] Braun, S., and J. A. Bottrel. Pilot study evaluating the effects of a cervical headgear on the C-axis: the growth axis of the dentomaxillary complex. American Journal of Orthodontics and Dentofacial Orthopedics, 126(6), 694-698, 2004.

[3] Brill, A. K., M. Moghal, M. J. Morrell, and A. K. Simonds. Randomized crossover trial of a pressure sensing visual feedback system to improve mask fitting in noninvasive ventilation. Respirology, 22(7), 1343-1349, 2017.

[4] Brill, A. K., R. Pickersgill, M. Moghal, M. J. Morrell, and A. K. Simonds. Mask pressure effects on the nasal bridge during short-term noninvasive ventilation. ERJ Open Research, 4(2), 00168, 2017.

[5] Dai, J., J. J. Yang, and Z. Zhuang. Sensitivity analysis of important parameters affecting contact pressure between a respirator and a headform. International Journal of Industrial Ergonomics, 41(3), 268-279, 2011.

[6] Gefen, A., and K. Ousey. Update to device-related pressure ulcers: SECURE prevention. COVID-19, face masks and skin damage. Journal of Wound Care, 29(5), 245-259, 2020.

[7] Hibbitt, H. D., Karlsson, B., and P. Sorensen. ABAQUS User's manuals. Release 2020, Simulia/Dassault Systemes, Providence, RI, USA, 2020.

[8] Kushida, C. A., M. R. Littner, M. Hirshkowitz, T. I. Morgenthaler, C. A. Alessi, D. Bailey, B. Boehlecke, T. M. Brown, J. Coleman, Jr., L. Friedman, S. Kapen, V. K. Kapur, M. Kramer, T. Lee-Chiong, J. Owens, J. P. Pancer, T. J. Swick, and M. S. Wise. Practice parameters for the use of continuous and bilevel positive airway pressure devices to treat adult patients with sleep-related breathing disorders. Sleep, 29(3), 375-380, 2006.

[9] Lei, Z., J. Yang, and Z. Zhuang. Headform and N95 filtering facepiece respirator interaction: contact pressure simulation and validation. Journal of Occupational and Environmental Hygiene, 9(1), 46-58, 2012.

[10] Lopomo, F. N., F. Savoldi, and F. Genna. Experimental determination of the contact pressures produced by a continuous positive airway pressure mask. To appear, 2021.

[11] Ma, Z., P. Hyde, M. Drinnan, and J. Munguia. Development of a smart-fit system for CPAP interface selection. Proceedings of the Institution of Mechanical Engineers, Part H: Journal of Engineering in Medicine, 235(1), 44-53, 2021.

[12] McEvoy, R. D., N. A. Antic, E. Heeley, Y. Luo, Q. Ou, X. Zhang, R. D. McEvoy, N. A. Antic, E. Heeley, Y. Luo, Q. Ou, X. Zhang, O. Mediano, R. Chen, L. F. Drager, Z. Liu, G. Chen, B. Du, N. McArdle, S. Mukherjee, M. Tripathi, L. Billot, Q. Li, G. Lorenzi-Filho, F. Barbe, S. Redline, J. Wang, H. Arima, B. Neal, D. P. White, R. R. Grunstein, N. Zhong, and C. S. Anderson. CPAP for prevention of cardiovascular events in obstructive sleep apnea. New England Journal of Medicine, 375(10), 919-931, 2016.

[13] Nightingale, R., N. Nwosu, F. Kutubudin, T. Fletcher, J. Lewis, F. Frost, K. Haigh, R. Robinson, A. Kumar, G. Jones, D. Brown, M. Abouyannis, M. Beadsworth, P. Hampshire, S. Aston, M. Gautam, and H. Burhan. Is continuous positive airway pressure (CPAP) a new standard of care for type 1 respiratory failure in COVID-19 patients? A retrospective observational study of a dedicated COVID-19 CPAP service. BMJ Open Respiratory Research, 7(1), e000639, 2020.

[14] Peko Cohen, L., Z. Ovadia-Blechman, O. Hoffer, and A. Gefen. Dressings cut to shape alleviate facial tissue loads while using an oxygen mask. International Wound Journal, 16(3), 813-826, 2019.

[15] Savoldi, F., J. K. H. Tsoi, C. Paganelli, and J. P. Matinlinna. The biomechanical properties of human craniofacial sutures and relevant variables in sutural distraction osteogenesis: a critical review. Tissue Engineering Part B: Reviews, 24(1), 25-36, 2018.

[16] Savoldi, F., B. Xu, J. K. H. Tsoi, C. Paganelli, and J. P. Matinlinna. Anatomical and mechanical properties of swine midpalatal suture in

the premaxillary, maxillary, and palatine region. Scientific Reports, 8(1), 1-12, 2018.

[17] Tsuda, H., F. R. Almeida, T. Tsuda, Y. Moritsuchi, and A. A. Lowe. Craniofacial changes after 2 years of nasal continuous positive airway pressure use in patients with obstructive sleep apnea. Chest, 138(4), 870-874, 2010.

[18] Worsley, P. R., G. Prudden, G. Gower, and D. L. Bader. Investigating the effects of strap tension during non-invasive ventilation mask application: a combined biomechanical and biomarker approach. Medical Devices (Auckland, NZ), 9, 409-417, 2016.

Reply to Reviewers (in red).

Reviewer: 1

Nothing to reply.

Reviewer: 2

1. All figures should be captioned with (a) and (b), instead of describing it as (left) and (right). Done.

2. Quantifying the amount of difference in the actual head gear contact compared to the computational model would be useful to give a sense of the source of variance in the pressure values. Unfortunately, no measurement of the pressures in the actual headgear was taken during the experiments, when the focus was on the contact pressures existing on the face of the dummy head.

3. How did the authors ensure symmetrical force loading, given the computational model was modelled using half the head due to symmetry. As apparent from the shown experimental setup, in both types of loading a theoretical symmetry did exist for both the geometries and the loading conditions. We did not take any special measure to go beyond the normal checks of these symmetries when loading the specimens, but we most certainly wanted to exploit them in the numerical models, where, even in the linear range, a doubling of the unknowns produces an increase by a factor of 8 of the computing time. During the experiments we did simply place the specimens in a centered position with respect to the machine heads. Considering the lack of space (see also point 9 later on, here) we felt this needed no new comments.

4. The upper lip pressure pad overlapped the symmetry line. This would cause some variances in the symmetry model. We do not understand this question. The setup of the pressure sensors was definitely not symmetric for space reasons, but this lack of symmetry of the sensors is not expected to produce any significant lack of symmetry in the measured pressures. Quite simply, the results in symmetric portions of the dummy head face, such as the upper lip one, came up almost identical to each other. This has no effects in terms of the predictions of symmetric numerical models.

5. Fig 3 could provide more views from different angles, and some zoomed views to allow the readers better insight into the setup. Done.

6. Fig 4 – the plots should use different colours for clear differentiation of the two variables. Done, also for Figures 5 and 7.

7. Fig 5 and 8 are very unclear. The right panel only shows some padding sections in the computational model. The left panel is experimental padding. The right paddle

show the contact pressure contour only but the face should be shown and since it is symmetrical the results for the entire face can still be shown. What is the definition of CPRESS SPOS? We believe the Reviewer means Figures 6 and 8, not 5 and 8. We have modified both figures to the best of our possibilities. The pressure contour plots are shown in this ABAQUS model only in the silicone rubber surfaces in contact with the face surface, which means that we needed to plot them removing the face surface and looking at the silicone rubber from the face side. Adding the head to this plot would completely cover the pressure contours. Therefore, we decided to add to this picture a sketch showing the position of the silicone parts with respect to the dummy head, to facilitate the comparison with the experimental results. We hope this is acceptable. CPRESS indicates contact pressures, as explained in the text. CPOS is just an ABAQUS output convention about the considered side of the surface, of no importance at all in this context. We have changed the legends anyway.

8. Table 1 shows the contact area are different. Therefore could the results be normalised with Force since Pressure = Force / Area. The total force applied to the dummy head face is here a datum, and it is the same in both the experimental and the numerical results, since it depends only on the force applied to the headgear. Therefore, we do not understand how the Table values could be normalized in any way. In any case, the interpretation of both the pressure values and the contact areas from FEM results in the presence of a 3D discrete surface is quite delicate anyway, as explained in the text.

9. There are no equations and there is a lack discussions of the numerical schemes, meshing, etc… used. For example why is a numerical damping coefficient a = -0.05 the best value to use? Are there citations for this? Agreed. But we may observe that (i) the topic hardly requires any equations to be introduced, and (ii) there is no space left for any deeper discussion about the meshes and/or the numerical schemes which are, in any case, fairly standard for the problem under study. Please consider that this Journal allows 5500 words everything included, and we are already beyond 6000. As for the α coefficient, this is standard in direct time integration theory and there is no space to refresh the criteria for its choice, which can be found in any Finite Element book (for example, Hughes' one); we have added a brief comment to it anyway.

10. Page 14 discusses some issues with shell elements, however the mesh design and selection of elements were not discussed in the Method. We already had comments about the choice both of shells and of the mesh at pages 5 and 8 of our manuscript. We have added a brief new one at page 8. Once again, we have no space for these issues here.

11. There is no conclusion section! How can a scientific paper be submitted without the correct scientific template/structure. Agreed, and very sorry about this, which is a mistake produced by our initial checking with the template of a different Journal which demanded no Conclusions section. We have added a new Conclusions section.

12. It is unclear what design changes would improve the mask fitting. We have added comments about this in the Conclusions section.